Interdomain Fluorescence Resonance Energy Transfer in SERCA Probed by Cyan-Fluorescent Protein Fused to the Actuator Domain[†]

Deborah L. Winters, Joseph M. Autry, Bengt Svensson, and David D. Thomas*

Department of Biochemistry, Molecular Biology, and Biophysics, University of Minnesota, Minneapolis, Minnesota 55455

Received October 17, 2007; Revised Manuscript Received February 11, 2008

ABSTRACT: We have used a biosynthetically incorporated fluorescent probe to monitor domain movements involved in ion transport by the sarcoendoplasmic reticulum Ca−ATPase (SERCA) from rabbit fast-twitch skeletal muscle. X-ray crystal structures suggest that the nucleotide-binding (N) and actuator (A) domains of SERCA move apart by several nanometers upon Ca binding. To test this hypothesis, cDNA constructs were created to fuse cyan-fluorescent protein (CFP) to the N terminus of SERCA (A domain). This CFP−SERCA fluorescent fusion protein retained activity when expressed in Sf21 insect cells using the baculovirus system. Fluorescence resonance energy transfer (FRET) was used to monitor the A−N interdomain distance for CFP−SERCA selectively labeled with fluorescein isothiocyanate (FITC) at Lys 515 in the N domain. At low $[Ca^{2+}]$ (E2 biochemical state), the measured FRET efficiency between CFP (donor in A domain) and FITC (acceptor in N domain) was 0.34 ± 0.03, indicating a mean distance of 61.6 ± 2.0 Å between probes on the two domains. An increase of $[Ca^{2+}]$ to 0.1 mM (E1−Ca biochemical state) decreased the FRET efficiency by 0.06 ± 0.03, indicating an increase in the mean distance by 3.0 ± 1.2 Å. Quantitative molecular modeling of dual-labeled SERCA, including an accurate calculation of the orientation factor, shows that the FRET data observed in the absence of Ca is consistent with the E2 crystal structure, but the increase in distance (decrease in FRET) induced by Ca is much less than predicted by the E1 crystal structure. We conclude that the E1 crystal structure does not reflect the predominant structure of SERCA under physiological conditions in a functional membrane bilayer.

The sarcoendoplasmic reticulum Ca−ATPase (SERCA)[1] is a 110 kDa integral membrane protein responsible for maintaining a 10 000-fold Ca gradient across the membrane of the sarcoplasmic reticulum (SR) in cardiac and skeletal muscle cells. SERCA couples the active transport of 2 mol of Ca/mol of ATP hydrolyzed during the enzymatic cycle. Early models of this cycle proposed that SERCA exists primarily in two biochemical states, namely, E1 and E2, or with and without bound Ca, respectively. Until recently, the structural basis for active Ca transport has been based on mutagenesis of Ca- and ATP-binding residues (1–5), low-resolution electron microscopy studies with bound ligands (6–12), and spectroscopic studies of intrinsic tryptophan (Trp) fluorescence and extrinsic optical and paramagnetic probes (13–17). Recent advances in X-ray crystallography of SERCA have refined the overall architecture of the protein, highlighting its four distinct functional domains (18–29): the nucleotide-binding (N), phosphorylation (P), actuator (A), and transmembrane (TM) domains. These X-ray crystal structures suggest domain rearrangements due to binding of ligands that stabilize intermediates of the SERCA catalytic cycle. In particular, the structures assigned to both the E1 (18) and E2 (19, 27, 28) biochemical intermediates show large differences, suggesting that the model of Ca binding at the transmembrane sites results in a dramatic rearrangement of the three cytosolic domains, most specifically between the A and N domains (Figure 1). These static crystal structures suggest the necessity for a large conformational transition between the E2 and E1 biochemical states. However, there is not necessarily a direct correspondence between structural states, defined by crystal structures, and biochemical states, defined by ligand concentrations under more physiological conditions. The E1 crystal structure was obtained at an extremely high Ca concentration (10 mM, 100-fold higher than needed for saturation of the high-affinity Ca-binding sites of SERCA) (30), and the E2 crystal structures have only been obtained when stabilized with the SERCA inhibitors: thapsigargin (Tg), cyclopiazonic acid (CPA), and 2,5-di(tert-butyl)-1,4-benzohydroquinone (BHQ) (19, 27, 28, 31). Thus, the question remains whether the

[1] Abbreviations: SERCA, sarcoendoplasmic reticulum Ca−ATPase; Ca, divalent calcium ion (Ca^{2+}); Mg, divalent magnesium ion (Mg^{2+}); AMPPCP, adenylylmethylenediphosphonate disodium salt; ProtK, proteinase K; FITC, fluorescein-5-isothiocyanate (FITC isomer I); DMF, dimethylformamide; Tg, thapsigargin; CFP, cyan-fluorescent protein; mCFP, monomeric cyan-fluorescent protein with an A206K mutation to eliminate dimerization; DIC, differential interference contrast; SDS−PAGE, sodium dodecyl sulfate−polyacrylamide gel electrophoresis; MOPS, 3-(N-morpholino)propanesulfonic acid; MES, 2-(N-morpholino)ethanesulfonic acid; TCA, trichloroacetic acid; $C_{12}E_8$, octaethylene glycol monodecyl ether; EGTA, ethyleneglycol-bis-(2-aminoethyl ether)N,N,N,N-tetraacetic acid; FRET, fluorescence resonance energy transfer; WT, wild type; MOI, multiplicity of infection; EPR, electron paramagnetic resonance.
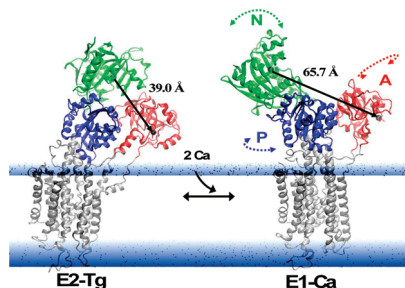
FIGURE 1: Model showing the effects of Ca binding on SERCA cytosolic domain movements. Based on X-ray crystal structures E2−Tg [1IWO (*19*)] and E1−Ca [1SU4 (*18*)]. Distances shown (in angstroms) are between the carbon α atoms of the FITC-labeling site Lys 515 and Met 1.

crystallographic data reflect the SERCA structures actually present during the Ca transport cycle in a biological membrane.

Spectroscopic techniques, such as fluorescence and electron paramagnetic resonance (EPR), are well-suited for making structural measurements in noncrystalline samples. For example, Ca binding to the high-affinity (micromolar) Ca-binding sites in the TM domain of SERCA in SR membranes causes a 5% increase in intrinsic Trp fluorescence (*32, 33*), probably due to changes in the local environments of Trp residues in the transmembrane domain. In the cytoplasmic headpiece, fluorescein isothiocyanate (FITC), attached specifically to Lys 515 in the N domain, undergoes a 5% decrease in fluorescence intensity upon micromolar Ca binding, suggesting long-range conformational coupling between the TM and N domains (*34, 35*). Similarly, the EPR spectrum of an iodoacetamide spin label, attached to Cys 674 in the P domain, shows that the rotational freedom of the probe changes slightly in response to Ca but more dramatically in response to ATP (*16*). Unfortunately, measurements of fluorophore emission and spin-label mobility do not provide direct information about the magnitude of a structural transition. In contrast, fluorescence resonance energy transfer (FRET) can directly detect molecular distance changes with high precision. Research from this laboratory and elsewhere has shown that FRET between the N and P domains is insensitive to Ca binding, as determined using multiple donor and acceptor labeling strategies (*13–15, 36, 37*). Collectively, these data show that Ca binding produces relatively small-scale structural changes within the cytosolic domain of SERCA, from the perspective of the N and P domains.

This conclusion was supported upon publication of the crystal structures assigned to the E1 (*18*) and E2 (*19, 27, 28*) biochemical states of SERCA, which showed that the N−P interdomain distance does not differ substantially between these structures. Rather, the crystal structures suggest that the largest Ca-induced structural change in the cytosolic domain of SERCA occurs in separation of the N and A domains. Indeed, the crystallographic data indicate an increase of about 27 Å in the distance between the N terminus of the A domain and the FITC-binding site at Lys 515 on the N domain (Figure 1).

One challenge to studying A-domain dynamics is that no specific native labeling sites have been identified on this domain. In the present study, we have created a novel labeling site on the A domain by covalently linking cyan-

fluorescent protein (CFP) to the N terminus of SERCA. With the baculovirus expression system, we show that overexpression of the fusion protein produces high quantities of active protein for biochemical and spectroscopic studies. Using CFP as the fluorescent donor and FITC attached to Lys 515 as the acceptor, we have used FRET to measure the A−N interdomain distance in response to Ca binding. Quantitative molecular modeling of the fluorophore movements within the fusion protein allowed us to compare the observed movement with those predicted by crystallographic models.

MATERIALS AND METHODS

Reagents and Solutions. Molecular biology enzymes were from New England Biolabs. Thapsigargin, AMPPCP, proteinase K, and other chemicals were of the highest grade and purity from Sigma-Aldrich.

Construction of SERCA Baculovirus Transfer Plasmids. The full-length wild-type (WT) SERCA1a cDNA from rabbit fast-twitch skeletal muscle was amplified by the polymerase chain reaction (PCR) from pBluescript and inserted into the *Sac* I and *Sma* I sites of the baculovirus transfer vector pAcSG2 (BD Biosciences, San Jose, CA), to yield pWT−SERCA (*38*). The cDNA encoding enhanced CFP was amplified by PCR from peCFP (Clontech, Mountain View, CA) and inserted in frame at the *Xho* I and *Sac* I sites of the pWT-SERCA vector (to yield pCFP−SERCA). The resultant vector, pCFP−SERCA, encoded a fluorescent fusion protein with CFP first, leading into the N terminus of SERCA, connected by a short intervening linker, Gly-Glu-Leu, between the two proteins. Site-directed mutagenesis with the QuikChange site-directed mutagenesis kit (Stratagene, La-Jolla, CA) was used to introduce an Ala to Lys mutation at residue 206 (A206K) into the CFP coding sequence to suppress CFP dimerization (pmCFP−SERCA) (*39*). All cDNA gene constructs were confirmed by dideoxy sequencing.

Recombinant SERCA Expression and Purification. SERCA proteins were expressed in Sf21 insect cells using the baculovirus expression system as described previously (*40*). Recombinant baculoviruses encoding WT−SERCA, CFP−SERCA, and mCFP−SERCA (referred to as CFP−SERCA throughout text unless otherwise noted) were created using the BaculoGold cotransfection kit (BD Biosciences, San Jose, CA). Recombinant SERCA proteins were isolated in Sf21 microsomal membranes using nitrogen cavitation and differential centrifugation (*40*). Microsomal membranes were flash-frozen in liquid nitrogen and stored at −80 °C. To determine total SERCA composition of the Sf21 microsome preparations, protein concentrations were measured and samples were subjected to sodium dodecyl sulfate−polyacrylamide gel electrophoresis (SDS−PAGE) analysis as described below.

LSR Purification. Light SR (LSR) vesicles were isolated from fast-twitch skeletal muscle of New Zealand white rabbits by differential centrifugation, followed by purification on a discontinuous sucrose gradient to remove heavy SR vesicles (*15, 41*). Samples were resuspended in sucrose buffer [300 mM sucrose and 30 mM 3-(*N*-morpholino)propanesulfonic acid (MOPS) at pH 7.0], then flash-frozen, and stored at −80 °C. The SERCA concentration was determined as the product of protein concentration and the fractional

concentration of SERCA, as determined from SDS−PAGE analysis (described below).

FITC Labeling and Stoichiometry. LSR vesicles and recombinant SERCA microsomes were selectively labeled with the lysine-reactive probe FITC (Molecular Probes, Eugene, OR) at Lys 515 in labeling buffer (100 mM KCl, 5 mM MgCl$_2$, and 30 mM Tris at pH 8.9), as described previously (*15*). The FITC concentration was first measured from the absorbance of a stock solution in dimethylforma- mide (DMF), using the extinction coefficient of 76 500 M^{-1} cm^{-1} of the manufacturer (494 nm, pH 9.0). The concentra- tion of SERCA-bound FITC was determined using an extinction coefficient of 63 000 M^{-1} cm^{-1} (at pH 7.0) (*15*). Specificity of labeling was verified by SDS−PAGE analysis as described below.

Gel Densitometry and Fluorescence Image Analysis of SDS−PAGE. Protein concentrations for all SERCA prepara- tions were determined by the Lowry method (*42*), using bovine serum albumin as a standard. Analysis of protein content and specificity of FITC labeling was achieved by electrophoresis of sample preparations through 4–20% Tris- HCl gradient gels (Bio-Rad, Hercules, CA). Gels were stained with Coomassie Brilliant Blue (R-250) or directly imaged for fluorescent-labeling analysis. Coomassie-stained images were acquired using a Bio-Rad GS-700 imaging densitometer, and lane-scan profiles were collected and analyzed for total WT−SERCA (110 kDa) or CFP−SERCA (140 kDa) content using the Bio-Rad Molecular Analyst (version 21) software. To assay FITC-labeling specificity, gels were excited at 450 ± 30 nm, FITC emission was detected through a 520 nm long pass filter using a STORM 860 gel imaging system, and lane-scan profiles were analyzed for fluorescence intensity using the analysis software ImageQuant (Molecular Dynamics, Sunnyvale, CA).

Ca-Dependent ATPase Measurements. ATP hydrolysis catalyzed by SERCA was measured using a NADH-coupled enzyme reaction in a microtiter plate as described previously (*17, 43*). The Ca concentration was controlled by a Ca/ ethyleneglycol-bis-(2-aminoethyl ether)*N,N,N,N*-tetraacetic acid (EGTA) buffering system (*44*). LSR vesicles were resuspended at 3 μg/mL, and SERCA-expressing microsomes were resuspended at 5–10 μg/mL in 200 μL of assay buffer (5 mM MgCl$_2$, 100 mM KCl, 1 mM EGTA, 0.4 mM NADH, 1.0 mM phosphoenolpyruvate, 5.0 mM ATP, 10 IU/mL lactate dehydrogenase, 10 IU/mL pyruvate kinase, 5 mM NaN$_3$, 7 μg/mL calcimycin A23187, and 50 mM MOPS at pH 7.0), and ATPase activity was measured from pCa 5.0−8.0 at 25 °C. The rate of ATP hydrolysis was deter- mined as the rate of [NADH] decrease, measured from absorbance at 340 nm using a Molecular Devices SpectraMax Plus (Sunnyvale, CA) spectrophotometer. The Ca dependence of ATPase activity was determined by fitting the data to the Hill equation,

$$V = \frac{V_{max}}{1 + 10^{-n(pK_{Ca} - pCa)}} \quad (1)$$

where V is the initial ATPase rate, n is the Hill coefficient, V_{max} is the value of V at saturating [Ca^{2+}], and $pK_{Ca} = -\log[K_{Ca}]$, where K_{Ca} is the value of Ca^{2+} at which $V/V_{max} = 0.5$.

Microscopy. Approximately 5.0 × 10^5 Sf21 cells were plated on 35 mm glass-bottom culture dishes (MatTek

Corporation, Ashland, MA) and were infected with SERCA viruses at a multiplicity of infection (MOI) of 10. Cells were imaged 48 h after infection using a TE-200 Nikon Eclipse (Nikon, Melville, NY) inverted microscope. CFP was excited using the X-Cite120 fluorescence illumination system (EXFO Photonics, Quebec, Canada) and a bandpass excitation filter with a 436 nm wavelength. Fluorescence emission was detected using a 460–500 nm dichroic filter. All images were captured using a 100× oil immersion objective (NA, 1.3) and a Photometrics Cascade II electron-multiplication, 16- bit CCD camera cooled to –80 °C. Image overlays were created using MetaMorph 7.0 image analysis software (Molecular Devices, Sunnyvale, CA).

Proteolysis of LSR and Microsomal Membranes. SERCA samples were tested for conformation-specific cleavage by proteinase K (ProtK) as a diagnostic test for protein folding and conformational sensitivity to ligand binding (*45, 46*). Approximately 20 μg of LSR and 40 μg of WT−SERCA or CFP−SERCA microsomal membranes were suspended in either E1 buffer (0.1 mM CaCl$_2$, 50 mM NaCl, 1.0 mM β-mercaptoethanol, and 50 mM MOPS at pH 7.0), E2 buffer (20 mM EGTA, 50 mM NaCl, 1.0 mM β-mercaptoethanol, and 50 mM MOPS at pH 7.0), or E1.N buffer (E1 buffer plus 1 mM AMPPCP). ProtK was added in a 1:20 (weight/ weight) ratio of ProtK/total protein and incubated for 15 min at 25 °C. Reactions were terminated by the addition of 2.5% (w/v) ice-cold TCA. ProtK digestion was also carried out at pH 7.0 in the presence of 3 mM MgCl$_2$ and at pH 6.0 with and without 3 mM MgCl$_2$ (data not shown). Approximately 20 μg of each sample was analyzed by SDS−PAGE as described above and visualized by fluorescence and/or Coomassie staining.

Fluorescence Measurements and Data Analysis. Fluores- cence spectra were obtained with an ISS-K2 fluorescence spectrophotometer (ISS, Champaign, IL), using a Xenon lamp as an excitation source at 25 °C. The excitation wavelength was 420 nm, which was chosen to maximize CFP excitation, with relatively weak FITC excitation. Emis- sion spectra were recorded from 450 to 600 nm in 2 nm increments. FRET was measured at an emission wavelength of 480 nm, near the peak of CFP emission, where FITC emission is negligible. CFP−SERCA (donor only), FITC- labeled WT−SERCA (acceptor only), or FITC-labeled CFP−SERCA (donor plus acceptor) samples were diluted into a quartz cuvette (1 cm path length) to a final concentra- tion of 100 μg/mL in 100 mM KCl, 25 mM MOPS (pH 7.0), plus either 0.1 mM CaCl$_2$ (E1 buffer) or 0.1 mM CaCl$_2$ and 2.0 mM EGTA (E2 buffer). A background spectrum of unlabeled Sf21 microsomes, at the same protein concentra- tion, was subtracted from the spectrum of labeled Sf21 microsomes to yield the reported fluorescence emission spectrum. The SERCA concentration was approximately 50 nM, resulting in absorbances of donor and acceptor below 0.01; thus, there was no need to correct for the inner-filter effect.

The FRET efficiency (E) was calculated as the fractional decrease of donor fluorescence (F_D) in the presence of acceptor (F_{DA}), according to

$$E = 1 - (F_{DA}/F_D) \quad (2)$$

The distance R between the CFP (donor) chromophore and the FITC (acceptor) probe was calculated from E according to

$$E = 1/[1 + (R/R_0)^6]$$
$$R = R_0[E^{-1} - 1]^{1/6} \tag{3}$$

where the Förster distance R_0 was calculated from

$$R_0 = 9780[J(\lambda)\kappa^2\eta^{-4}\varphi_D]^{1/6} \tag{4}$$

where κ^2 is the orientation factor (assumed to be $^2/_3$ for random orientation), η is the index of refraction of the medium (1.4), and φ_D is the donor quantum yield [0.40 for CFP (47)]. $J(\lambda)$ is the spectral overlap integral between CFP and FITC, which was calculated from the donor emission spectrum [$F_D(\lambda)$] and the acceptor excitation [$\varepsilon_A(\lambda)$] according to

$$J(\lambda) = \frac{\int F_D(\lambda)\,\varepsilon_A(\lambda)\,\lambda^4\,d\lambda}{\int F_D(\lambda)\,d\lambda} \tag{5}$$

and numerical integration using a Microcal Origin 7.0 template written by Igor Negrashov. The calculated R_0 value for CFP and FITC (assuming $\kappa^2 = {}^2/_3$) is 55 ± 1 Å.

Upper and lower limits on κ^2 and R_0 were determined from the steady-state fluorescence anisotropies of the donor and acceptor, as described previously (48, 49). Steady-state fluorescence anisotropy was measured for samples containing only the donor (CFP−SERCA) or acceptor (FITC-labeled WT−SERCA). Anisotropy, $r = (I_v - I_h)/(I_v + 2I_h)$, was measured by excitation (410 nm for CFP and 460 nm for FITC) with vertically polarized light, with emission (510 nm for CFP and 520 nm for FITC) detected through a polarizer oriented either vertically (I_v) or horizontally (I_h).

The most important experimentally determined value in this study was the change in energy-transfer efficiency ΔE corresponding to the E2−E1 transition (i.e., due to the addition of Ca). Therefore, each value of ΔE was determined pairwise by dividing a single sample in two, then adding a small volume of either Ca (to produce E1 buffer) or EGTA (to produce E2 buffer), and calculating $\Delta E = E(E1) - E(E2) = [F_{DA}(E1) - F_{DA}(E2)]/F_D$. F_D was found to be unaffected by Ca addition, and the standard error of the mean (SEM) for ΔE, determined in this pairwise fashion, was smaller than the sum of SEM values for $E(E1)$ and $E(E2)$, evaluated independently.

Molecular Modeling of CFP−SERCA. To simulate and interpret FRET experiments, fusion proteins were constructed *in silico* using atomic coordinates for the structures of SERCA in the E2−Tg [PDB ID: 1IWO (19)] and E1−Ca [PDB ID: 1SU4 (18)] conformations and the crystal structure of CFP [PDB ID: 1RM9 (50)] using the molecular modeling software packages DS Visualizer (Accelrys, San Diego, CA) and Fusion Protein Modeler (FPMOD) (51, 52). The first two residues of the SERCA structures were reoriented by torsional rotation to allow for the attachment of CFP at the N terminus. The three amino acids (Gly-Glu-Leu) that resulted from the subcloning of the two cDNA molecules were modeled onto the N terminus of SERCA to ensure that the *in silico* protein was identical to the expressed fusion protein used to acquire experimental data. The residues missing from the X-ray crystal structure of CFP at the N

(Val-Ser) and C (Thr-Leu-Gly-Met-Asp-Glu-Leu-Tyr-Lys) termini were added to its *in silico* structure and then attached to the N terminus of SERCA. Each structure was inserted into a lipid bilayer prior to structure simulation.

To simulate the multitude of possible conformations that CFP can adopt with respect to SERCA in solution, we created an ensemble of structural models for both E1−CFP−SERCA and E2−CFP−SERCA. Using the software FPMOD, the SERCA and CFP structures were treated as rigid bodies joined by a flexible linker region that was allowed to rotate freely. The nine C-terminal residues of CFP, which are unresolved and assumed to be flexible in the crystal structure and the first residue of the GEL sequence at the N terminus of SERCA were assigned to be part of this flexible linker. Structures where the CFP or linker sequence became positioned in the membrane bilayer were excluded from the ensembles using the assumption that the membrane has a total thickness of 45 Å and that these structures were energetically unfavorable and unlikely to reflect possible *in vitro* conformations. As a final step, the fluorescent label FITC at Lys 515 and the CFP chromophore were modeled into the structures using the McLachlan fitting algorithm as implemented in the program ProFit (Martin, A. C. R., http://www.bioinf.org.uk/software/profit/). Multiple conformations for FITC at Lys 515 were sampled by torsional rotations for every structure in each ensemble. Molecular visualization and creation of structural figures were accomplished using the software VMD (53).

Simulation of FRET Parameters from Molecular Modeling Data. For each structure, we calculated both the distance between the centers of the two chromophores (R) and the Förster distance (R_0). To calculate R_0, the orientation factor κ^2 was calculated explicitly from the observed probe orientations using dynamic reorientation averaging based on order parameters from anisotropy measurements (49)

$$\kappa^2 = \kappa_o^2 S_D S_A + (1 - S_D)/3 + (1 - S_A)/3 +$$
$$\cos^2\theta_D S_D(1 - S_A) + \cos^2\theta_A S_A(1 - S_D)$$

where

$$\kappa_o^2 = (\cos\theta_T + 3\cos\theta_D\cos\theta_A)^2 \tag{6}$$

θ_D and θ_A are the angles between the interprobe vector and the donor and acceptor transition moments, respectively, and θ_T is the angle between these two transition moments. S_D ($r_D = 0.33$) and S_A ($r_A = 0.27$) are the order parameters determined from the steady-state anisotropies r of the donor
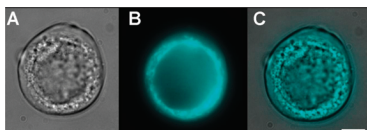
FIGURE 2: Imaging of CFP−SERCA in live Sf21 cells. Shown is a representative cell expressing CFP−SERCA. (A) DIC. (B) Epifluorescence. (C) Overlay. Images were acquired using a 100× oil immersion objective. Scale bar = 10 μm.

and acceptor, respectively, according to $S = (r/0.4)^{1/2}$. R_0 was then calculated for each simulated structure from

$$R_0(\kappa) = R_0(2/3) \times (3\kappa/2)^{1/3} \qquad (7)$$

where $R_0(2/3) = 55$ Å (eq 4). This allowed us to calculate not only the predicted distribution of distances (R) but also the predicted values of measured energy-transfer efficiency (E), using eq 3. Transition dipole moments for the CFP and FITC chromophores were adopted by analogy from published data (*54, 55*).

RESULTS

Baculovirus Expression of SERCA Proteins in Sf21 Cells. The baculovirus system has been used extensively for expression of SERCA in insect cells, providing milligram quantities of recombinant protein with preservation of near-native activity (*40, 56–58*). In the present study, we expressed three SERCA constructs in Sf21 insect cells: wild-type SERCA (WT−SERCA), SERCA with CFP fused to the N terminus (CFP-SERCA), and SERCA with monomeric CFP (containing the A206K mutation to suppress dimerization) fused to the N terminus (mCFP−SERCA). Essentially, all experiments in this study were carried out with both CFP−SERCA and mCFP−SERCA, with no significant differences in expression level, ATPase activity, or FRET, and are referred to below as CFP−SERCA unless otherwise noted. Figure 2 shows a live Sf21 cell expressing recombinant CFP−SERCA 48 h after infection with baculovirus. Differential interference contrast (DIC) microscopy (Figure 2A) shows the enlarged nucleus of the cell; a hallmark of infection with baculovirus. Epifluorescence microscopy (Figure 2B) reveals the perinuclear expression of CFP−SERCA in the endoplasmic reticulum (ER) of the infected cell. An image overlay (Figure 2C) demonstrates that the SERCA fluorescent fusion protein is specifically targeted to the ER membranes of Sf21 insect cells.

Microsomal membranes highly enriched in ER vesicles were isolated from infected cells for biochemical and biophysical characterization of CFP−SERCA. Sf21 microsomes containing recombinant SERCA proteins were subjected to SDS−PAGE, followed by fluorescent visualization and Coomassie staining (Figure 3). Expressed WT−SERCA migrated at its expected molecular weight of 110 kDa, and CFP−SERCA migrated at 140 kDa, as expected upon addition of the 30 kDa CFP fusion partner (lanes 2 and 3 in Figure 3A). Recombinant SERCA proteins were overexpressed at 5–20% of the total microsomal fraction for each protein, as revealed by quantitative densitometry of Coomassie Blue stained bands. Typically, the microsomal fractions of CFP−SERCA and mCFP−SERCA expressed at approximately twice the level of WT−SERCA (Table 1).
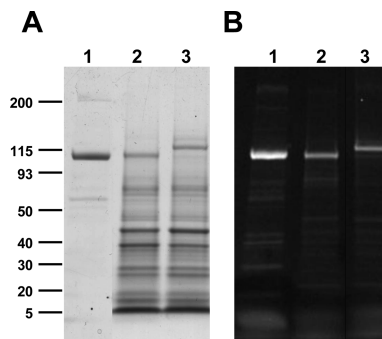

FIGURE 3: Expression and FITC labeling of SERCA proteins in Sf21 microsomes as detected by SDS−PAGE. (A) Coomassie. (B) Fluorescence. LSR (lane 1), WT−SERCA (lane 2), and CFP−SERCA (lane 3). A total of 25 μg of microsomal protein was loaded per lane. Excitation was at 450 ± 30 nm. Emission was detected using a 520 nm long-pass filter. Molecular weights based on standards are shown on the left in kilodaltons.
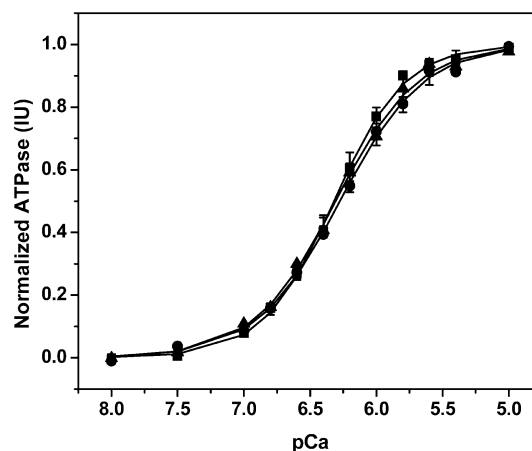

FIGURE 4: ATPase activity of SERCA in membrane vesicles. LSR (■), WT−SERCA (▲), and mCFP−SERCA (●). Values are normalized to V_{max} and shown as mean ± SEM ($n = 4$). Curves show fits of eq 1, yielding pK_{Ca} values of 6.30 ± 0.03, 6.31 ± 0.03, and 6.27 ± 0.04, respectively.

Ca-Dependent ATPase Activity. To determine whether the WT−SERCA and CFP−SERCA proteins were catalytically active, Sf21 microsomes were assayed for Ca-dependent ATPase activity at 25 °C in the presence of Ca ionophore (A23187), as described previously (*43*). Recombinant WT−SERCA showed high Ca−ATPase activity, similar to that of native SERCA in LSR, and the fusion proteins CFP−SERCA and mCFP−SERCA displayed 40–50% of the Ca−ATPase activity of recombinant WT−SERCA (Table 1). For both recombinant preparations, the Ca dependence of ATPase activity was virtually identical to that of LSR (Figure 4), demonstrating that the CFP-modified enzyme undergoes the same Ca-dependent structural transitions as WT−SERCA during the reaction cycle. Introduction of the A206K mutation in CFP to suppress dimerization had no significant effect on the ATPase activity of the enzyme but eliminated the aggregation occasionally seen on SDS−PAGE (data not shown).

FITC Labeling. Previous reports show that FITC stoichiometrically modifies residue Lys 515 in the nucleotide-binding pocket and completely inhibits the ATPase activity of the enzyme (*35, 59*). Here, we found that FITC labeling also eliminated more than 98% of Ca−ATPase activity by WT−SERCA, CFP−SERCA, and mCFP−SERCA in Sf21
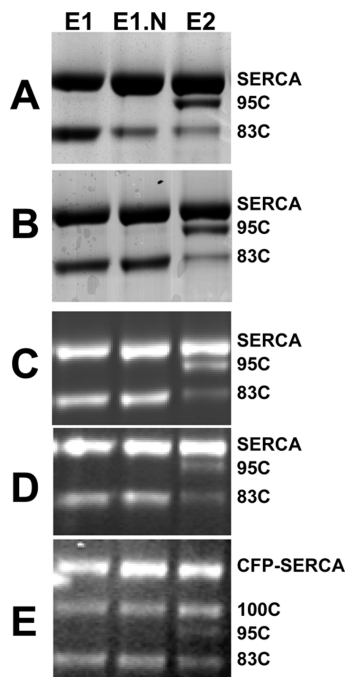
FIGURE 5: ProtK digestion analyzed by SDS−PAGE. (A) LSR. (B and C) LSR labeled with FITC. (D) WT−SERCA labeled with FITC. (E) CFP−SERCA labeled with FITC. (A and B) Coomassie. (C−E) fluorescence. Lanes are labeled according to buffers during digestion, as defined in the Materials and Methods.

FIGURE 6: Spectral overlap used to determine R_0. The donor emission spectrum (—, normalized to maximum) was obtained from microsomes containing CFP−SERCA. The acceptor absorbance spectrum (- - -) was obtained from microsomes containing FITC-labeled WT−SERCA. R_0 was calculated to be 55 ± 1 Å.

microsomes (data not shown), indicating that the recombinant enzyme is completely labeled by FITC, with similar results as the native enzyme. Fluorescence gel imaging and densitometry determined that >85% of the dye was bound to SERCA, whether in LSR membranes or Sf21 microsomes (Figure 3B). Quantitative analysis of the [dye]/[SERCA] labeling ratio, determined from dye absorbance of solubilized membranes and the SERCA content in the same membranes, showed that 0.9−1.2 mol of FITC was bound/mol of SERCA, in LSR as well as in Sf21 microsomes expressing WT−SERCA or CFP−SERCA. We conclude that Lys 515 is completely and specifically labeled with FITC, the FRET acceptor.

Proteolysis of SERCA Proteins by ProtK. To further characterize protein folding and conformational response to ligand binding by recombinant SERCA expressed in insect cells, Sf21 microsomes were digested with ProtK and analyzed by SDS−PAGE. Native SERCA in LSR shows conformation-specific digestion by ProtK (*45, 46, 60*). The main cleavage sites for ProtK are located between Leu 119−Lys 120 and Thr 242−Glu 243, resulting in a 95 kDa C-terminal fragment (95C) or a 83 kDa C-terminal fragment (83C), respectively (*61*). It has been shown that the relative rates of cleavage at these two sites reveal conformational changes due to Ca and nucleotide binding (*45, 46, 60–62*), as confirmed in Figure 5A. Digestion of LSR in the presence of Ca (E1) produces the 83C fragment; this cleavage is partially inhibited by AMPPCP binding (E1.N) and is further reduced by Ca removal (E2), where the 95C fragment is observed. FITC labeling (parts B and C of Figure 5) blocks the effect of AMPPCP (E1.N), confirming that FITC blocks nucleotide binding but not the effect of Ca removal (E2), indicating clearly that FITC does not mimic either the effect of nucleotide binding or Ca release. The pattern of proteolytic
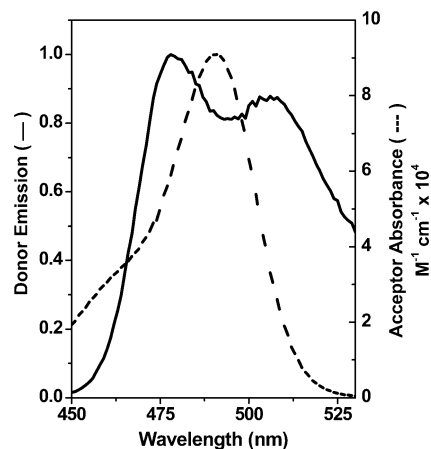
susceptibility was similar for FITC-labeled WT−SERCA and CFP−SERCA in Sf21 microsomes (compare parts D and E in Figure 5), indicating that the fluorescent fusion protein undergoes similar conformational changes as the WT enzyme in response to ligand binding. The additional 100 kDa band (100C) in Figure 5E is a result of ProtK cleavage of CFP from the fusion protein. ProtK digests for the E1, E1.N, and E2 biochemical states were conducted at pH 6.0 and 7.0, both with and without Mg, yielding results indistinguishable from those presented in Figure 5 (data not shown). We conclude that the samples used for FRET in the present study undergo similar Ca-dependent conformational changes as in WT−SERCA with and without bound FITC.

FRET Measurements within FITC-Labeled CFP−SERCA. Figure 6 illustrates the excellent spectral overlap between the donor (CFP) emission and the acceptor (FITC) excitation in samples prepared from insect microsomes. Using eq 4, the R_0 value for this pair was calculated to be 55 ± 1 Å. FRET provides good sensitivity for measuring distances from $0.5R_0$ to $1.5R_0$ (*48*), corresponding to 30–80 Å in this case, a range corresponding well to interdomain distances predicted by the X-ray crystal structures of SERCA (Figure 1).

Upon excitation at 420 nm, microsomes expressing CFP−SERCA show high fluorescence, many times greater than controls, with an emission maximum at 480 nm and a shoulder at 512 nm, characteristic of CFP (Figure 6). FITC labeling of CFP−SERCA produced a decrease in CFP fluorescence (Figure 7), a clear indication of FRET between CFP (donor) in the A domain and FITC (acceptor) in the N domain, in both the presence and absence of Ca. Energy-transfer efficiency (E) was calculated using eq 2, and the apparent distance R between the two probes was calculated using eq 3. In the example shown in Figure 7, in the absence of Ca, the fractional decrease in donor fluorescence (arrows in A and C) corresponds to FRET efficiency $E = 33.6\%$ and an interprobe distance $R = 61.6$ Å. In the presence of Ca (arrows in B and D), $E = 24.6\%$ and $R = 66.3$ Å. The mean ($\pm$SEM) values of six trials (six preparations) were $E = 0.336 \pm 0.03$ and $R = 61.6 \pm 2.0$ Å for the calcium-free enzyme (E2) and $E = 0.277 \pm 0.02$ and $R = 64.6 \pm 1.4$ Å for the calcium-bound enzyme (E1). Pairwise analysis of the change due to Ca addition (E2−E1) resulted in greater

Table 2: Simulated and Experimental Energy-Transfer Efficiency (E) and Distance (R in Angstroms) between CFP- and FITC-Labeled SERCA in Sf21 Microsomes[a]

	E (simulated)[b]	E (experimental)[c]	R (simulated)[b]	R experimental)[c]
E1	0.140 ± 0.004	0.277 ± 0.020	81.7 ± 0.3	64.6 ± 1.4
E2	0.420 ± 0.007	0.336 ± 0.030	52.2 ± 0.2	61.6 ± 2.0
$\Delta E = E(E1) - E(E2)$	−0.280 ± 0.011	−0.059 ± 0.022[d]		
$\Delta R = R(E1) - R(E2)$			29.5 ± 0.5	3.0 ± 1.2[d]

[a] Errors are ± SEM. [b] Simulated data based on dynamic averaging of κ^2 values. [c] Experimental data based on the average of six experiments. [d] Significantly different from 0 ($p < 0.01$ by Student's t test).
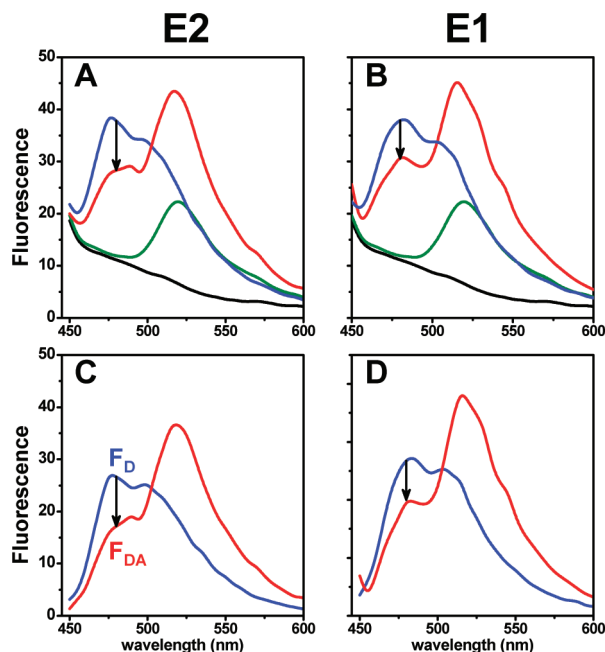

FIGURE 7: Representative fluorescence emission spectra. SERCA labeled with CFP (blue, donor, F_D), FITC (green, acceptor, F_A), both (red, F_{DA}), neither (black). E2 (Ca-free). E1 (Ca-bound). (Top) Raw data. (Bottom) After subtracting the black spectrum. Arrows indicate a decrease in donor fluorescence ($F_{DA} < F_D$) at the CFP emission maximum = 480 nm.

precision: $\Delta E(\text{Ca}) = 0.059 \pm 0.022$, and $\Delta R(\text{Ca}) = 3.0 \pm 1.2$ Å (Table 2). Thus, FRET results indicate that the distance between the A and N domains of SERCA changes only slightly in response to Ca binding. For a comparison, X-ray crystal structures indicate that the distance between the A and N domains increases by 27 Å upon Ca binding, nearly 10 times the observed change. We also tested the nucleotide effect on FRET between CFP and FITC, but as expected, AMPPCP (2.5 mM) had no effect on the FRET distance for FITC-labeled CFP−SERCA, presumably due to blockage of nucleotide binding by FITC in the N domain (data not shown).

Estimation of the Uncertainty due to Orientation. Upper and lower limits on κ^2 and R_o were determined from the steady-state fluorescence anisotropies of the donor and acceptor. The anisotropy of CFP−SERCA (donor) was measured to be 0.33 ± 0.02 (corresponding to an order parameter S_D of 0.91), in agreement with a previous report for GFP, for which the anisotropy was found to be independent of its linkage in a fusion protein (63). The anisotropy of FITC−SERCA was measured to be 0.27 ± 0.02 (corresponding to an order parameter S_A of 0.82). Both anisotropies were independent of Ca (same for E1 and E2). Based on these values, there is an 80% probability that the

actual distance R_{act} is related to the apparent distance R_{app} according to (48)

$$0.73 < R_{\text{act}}/R_{\text{app}} < 1.11 \qquad (8)$$

thus, the only likely substantial error is an overestimate of the distance, by as much as $1/3$. To reduce this uncertainty, we calculated the orientation factor quantitatively from molecular modeling, as described below.

FRET Simulations. To compare experimental FRET data with predictions from crystal structures, FRET experiments were simulated quantitatively based on molecular modeling of the CFP−SERCA fusion proteins. Molecular simulations were performed on the E2−CFP−SERCA and the E1−CFP−SERCA structures to determine a representative ensemble of CFP−SERCA conformations for each state. Approximately 5000 models were generated in the ensemble for the E2−CFP−SERCA and 4000 for E1−CFP−SERCA. These ensembles of models were further processed to remove structures where CFP overlapped with the membrane, because insertion of the soluble CFP protein into the membrane environment is assumed to be energetically unfavorable; there were 1173 models in the E2−CFP−SERCA ensemble and 1339 models in the E1−CFP−SERCA ensemble. Representative structures in each state are shown in Figure 8A.

After elimination of unlikely CFP−SERCA structures, multiple conformations for FITC modeled at the K515-binding site in each of the 1173 structures for E2−CFP−SERCA and 1339 structures for E1−CFP−SERCA were sampled by torsional rotations. For every model in each ensemble, the center positions and vectors for the CFP and FITC chromophore transition dipoles were calculated. The distance R and angles between dipoles were computed using these vectors, and subsequently, a dynamically averaged value for κ^2 was calculated using eq 6. The distribution of distances (R) between FITC and the CFP chromophore ranged from approximately 30 to 75 Å in the E2−CFP−SERCA structure, with a mean distance (±SEM) of 52.2 ± 0.2 Å (Figure 8B and Table 2). In the E1−CFP−SERCA structure, the distances ranged from about 50 to 110 Å, with a mean distance of 81.7 ± 0.3 Å. The distribution of E values, which is directly comparable to the experimental data, was calculated with eqs 4 and 6 (Figure 8C and Table 2). The mean E values (±SEM) for E2−CFP−SERCA and E1−CFP−SERCA are 0.420 ± 0.007 and 0.140 ± 0.004, respectively. Thus, while the simulations predict wide distributions of both R and E values, the SEM values are small and the simulated values for the E2 and E1 crystal structures differ much more than the experimentally observed values (Table 2). While the predicted change because of Ca addition is given by $\Delta E = -0.28 \pm 0.01$ and $\Delta R = 29.5 \pm 0.5$ Å, the experimentally observed change is much smaller: $\Delta E = -0.059 \pm 0.022$
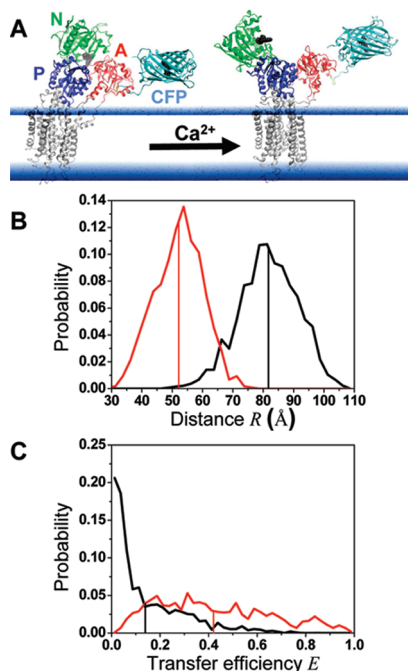
FIGURE 8: Simulated FRET parameters based on molecular modeling of CFP−SERCA. (A) Representative models of CFP−SERCA in the E2 and E1 states based on crystal structures [1IWO (*19*)] and [1SU4 (*18*)]. FITC at Lys 515 and the CFP chromophore are highlighted in the N domain and CFP molecule, respectively (black spacefill). Arrows indicate donor–acceptor distances. (B) Distance distribution. (C) Energy-transfer efficiency distribution. E2 (red) or E1 (black). Vertical lines indicate mean values. The mean values of *E* are the predicted experimental results.

and $\Delta R = 3.0 \pm 1.2$ Å. We considered other values for the mean orientation of the FITC probe bound to K515 (in addition to the most likely orientation based on modeling) and found that other orientations either gave results (distribution of *E*) that were similar to that reported in Figure 8 or showed even a greater discrepancy between the experimental and simulated *E* value for the E1 state.

DISCUSSION

Summary of Results. In the present study, we have used FRET to monitor SERCA cytosolic domain movements using a biosynthetically incorporated fluorophore to solve a long-standing problem in the SERCA field: the lack of specific labeling sites for spectroscopic probes on the A domain. Here, we fused CFP to the N terminus of SERCA through recombinant DNA technology, providing a unique fluorescent probe attached to the A domain (Figure 8). Expression of the CFP−SERCA fusion protein in Sf21 insect cells allowed us to monitor functional dynamics of the A domain in a biological membrane system under physiological conditions. FRET was used to measure distance changes within the fluorescent fusion protein, using CFP on the A domain as a donor and FITC on Lys 515 in the N domain as an acceptor. We found that the distance between CFP and FITC increased by only 3 ± 1 Å in response to Ca (Table 2), indicating that the A and N domains move slightly away from each other upon high-affinity Ca binding at the transmembrane sites in SERCA.

Relationship of FRET Results to X-ray Crystal Structures. X-ray crystallography has produced high-resolution structures of SERCA under a wide range of crystallization conditions,

which serve as models for possible structures that occur during the calcium transport cycle (*18–21, 23–29, 64*). Of particular interest here are the movements of the N, P, and A domains (comprising the cytosolic "headpiece") suggested to occur in response to Ca or nucleotide binding. The crystal structures of E1−Ca (1SU4), E2−Tg (1IWO), and E1−AMPPCP (1VFP) suggest that the N and P domains move relatively little with respect to each other in response to ligand binding, with interdomain distance changes less than 10 Å, while the most striking conformational changes in SERCA occur with the displacement of the A domain relative to the other two cytosolic domains. For example, the crystal structures of SERCA in the Ca-free (E2−Tg) and Ca-bound (E1−Ca) states predict that the distance between Met 1 in the A domain and Lys 515 in the N domain increases by 27 Å upon Ca binding (Figure 1). Here, we used FRET to measure directly the distance between CFP attached to the N terminus of the A domain and Lys 515 in the N domain, in active membranes, as a test of the X-ray crystal models (Figure 8). The results show that Ca binding increases the A−N domain distance by only 3 Å (Table 2), much less than the predicted 27 Å movement cited above.

It is not likely that this discrepancy arises from different buffer conditions in crystals and FRET samples. The E2−Tg crystal structure (1IWO) used in simulating the data (Figures 1 and 8) was obtained in the presence of thapsigargin (*19*), but no significant effect was observed in our E2 FRET experiment upon thapsigargin addition (data not shown). The E1−Ca crystal structure (1SU4) used in simulating the data (Figures 1 and 8) was obtained in the presence of 10 mM Ca (*18*), at least 1000-fold higher than required for SERCA activation, but no significant effect was observed in our E1 FRET experiments upon increasing $CaCl_2$ from 0.1 to 10 mM (data not shown).

It is not likely that this discrepancy arises from structural perturbations caused by attachment of the fluorescent probes. ProtK digestion of native SERCA shows that FITC labeling does not prevent the Ca-dependent transition from E2 to E1 nor does FITC cause the same conformational change (which includes closure of the SERCA headpiece) as AMPPCP binding (compare parts A and B of Figure 5). On the contrary, while FITC prevents AMPPCP binding (*35, 65*), it does this by blocking the effects of the nucleotide and not by mimicking them. Finally, FITC-labeled CFP−SERCA undergoes the same Ca-dependent transitions as FITC-labeled WT−SERCA (parts D and E of Figure 5).

It is not likely that this discrepancy is due to the uncertainty in the orientation factor (κ^2), which can cause a systematic error in R_0 and thus decreases the accuracy of the distance measurement (*48, 49*). Based on the measured fluorescence anisotropies of donor and acceptor, we determined that the primary uncertainty is that the distance may be overestimated, by as much as $1/3$ (eq 8). However, because the probe anisotropy is not Ca-dependent and *E* is a function of R/R_0 (eq 3), it is likely that the error would be similar in the presence and absence of Ca and the relative distances would still be accurate.

It is not likely that the discrepancy is due to mobility of CFP relative to the A domain. It is important to consider this possibility, because CFP is attached to the N terminus of SERCA via a 10-residue flexible linker. Therefore, we modeled the structures of CFP attached to the A domain and
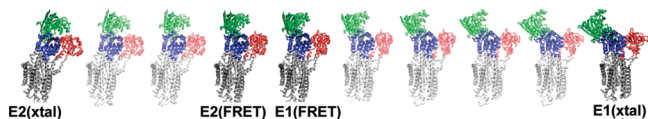
FIGURE 9: Ca-induced structural change in SERCA. The structures on the ends are crystal structures, E2−Tg [1IWO (*19*)] and E1−Ca [1SU4 (*18*)]. Between them is a series of evenly spaced intermediate structures, generated using the Yale Morph Server (http://molmovdb.org/molmovdb/morph) (*66*). "E2 (FRET)" and "E1 (FRET)" are the structures in this sequence that are most consistent with FRET results.

FITC attached to Lys 515 on the N domain (Figure 8) to obtain simulated distances to compare to our experimental data. The results show that, even when the simulations allow the linker to have virtually complete flexibility, resulting in a wide distribution of distances in both E2 and E1 states (Figure 8A), the predicted mean values of distance (*R*, Figure 8B) and FRET (*E*, Figure 8C) both change with Ca much less in the experiments ($\Delta E = -0.059 \pm 0.022$, and $\Delta R = 3.0 \pm 1.2$) than in the simulations ($\Delta E = -0.280 \pm 0.011$, and $\Delta R = 29.5 \pm 0.5$) (Table 2). Additionally, when FITC was allowed to adopt multiple conformations within the ATP-binding pocket, we found that many of these FITC orientations gave results (distribution of *E*) that suggest an even greater discrepancy between the experimental FRET data and the simulated data for the E1 state. We conclude that the E2 crystal structure, indicating close proximity of A and N domains, is slightly more closed than experimentally observed in the absence of Ca in active membranes and that the E1 crystal structure is much more open than experimentally observed in the presence of Ca (Table 2).

There are several alternative explanations for these results, as illustrated in Figure 9. The simplest explanation is that the structures of SERCA in the absence and presence of Ca are each distinct, ordered structures ["E2 (FRET)" and "E1 (FRET)" in Figure 9] that are similar to each other and to the closed E2−Tg crystal structure (1IWO) but quite different from E1−Ca (1SU4). However, it seems more likely that the E2−Tg and E1−Ca crystal structures are present but that their differences are partially obscured by structural dynamics. For example, the data are consistent with a model in which both E2−Tg and E1−Ca crystal structures are populated and Ca simply shifts the dynamic equilibrium toward E1−Ca. The energy-transfer efficiency in this case is given by

$$E = x_1 E(\text{E1}) + (1 - x_1) E(\text{E2})$$
$$x_1 = [E - E(\text{E2})]/[E(\text{E1}) - E(\text{E2})] \qquad (9)$$

where x_1 is the mole fraction of SERCA in the E1 crystal structure and $E(\text{E1})$ and $E(\text{E2})$ are the simulated *E* values given in Table 2. From Table 2, the value of x_1 is $30 \pm 1\%$ E1 in the absence of Ca and $51 \pm 1\%$ E1 in the presence of Ca. The data are also consistent with a highly flexible, dynamically disordered headpiece, in which many intermediate structures are populated, particularly in the presence of Ca (Figure 9). In fact, the model depicted in Figure 9, showing a continuum of equally populated structures, is predicted to give $E = 0.28$, almost exactly the energy-transfer value observed in the presence of Ca.

The N domain is a continuous polypeptide strand (approximately residues Glu 360−Arg 604) inserted within the sequence of the P domain (Asn 330−Asn 359 and Lys 605−Asp 737), creating a flexible "hinge" where the two domains are connected. Xu et al. (*67*) have proposed that this hinge flexibility renders the N domain susceptible to Brownian motion and that its orientational distribution could represent a random sampling of structures. The reported E1−Ca crystal structure (1SU4) with the wide A−N domain distance (i.e., "open" headpiece) could be one of many conformations accessible to SERCA prior to ATP binding. It has been noted that the E1−Ca structure could be distorted by crystal contacts between the N and A domains of one SERCA molecule with those of its nearest neighbor (*18, 68*). Our present findings indicate that the "open" headpiece with the wide A−N distance is not the predominant structure populated by E1−Ca under physiological conditions. Considering that concentrations of ATP and ADP within the cell are high enough to keep the nucleotide-binding site occupied at any given time, Jensen et al. (*69*) have proposed that the cytosolic headpiece of SERCA is "closed" during the entire catalytic cycle. Our FRET results indicate that nucleotide binding is not required for this compact structure but rather that the cytosolic headpiece of the E1 enzyme in fully hydrated lipid bilayers under physiological conditions is much more compact than that seen in the crystal structure.

Relationship to Previous Spectroscopic Data. This laboratory has previously reported a FRET study of SERCA structural dynamics using two well-characterized native labeling sites: FITC labeling of Lys 515 on the N domain and IAEDANS labeling of Cys 674 on the P domain (*15*). That study showed that there was no significant change in energy-transfer distance within the measured range (31 Å $\leq R_1 \leq 40$ Å) in response to Ca, phosphate, or vanadate binding. An examination of the E1−Ca (1SU4), E2−Tg (1IWO), and E1−AMPPCP (1VFP) crystal structures indicates that this finding is not surprising, because the distances between Lys 515 and Cys 674 do not vary by more than a few angstroms (Figure 1). Other FRET studies using a variety of labeling strategies have also demonstrated little or no change in distance between fluorescent probes in the N and P domains (as reviewed by ref *14*). These FRET results using native sites in SERCA were later corroborated by X-ray crystallography. We conclude that FRET is a useful and accurate tool to measure interdomain distances in SERCA.

Spectroscopic Probes of SERCA Domain Dynamics. Previously, we reported EPR and time-resolved phosphorescence anisotropy studies that probed the effects of Ca and ATP binding on domain dynamics (*16, 17*). Consistent with the present results, the effects of Ca binding were subtle. EPR of a spin label bound to SERCA at Cys 674 showed significant changes in the nanosecond internal dynamics of the SERCA P domain in response to Ca plus ATP but not Ca alone (*16*). Similarly, time-resolved phosphorescence anisotropy showed that ATP binding affects P domain microsecond dynamics and membrane tilt, while Ca has only very minor effects (*17*). Detection of the effects of nucleotide binding on FRET between A and N domains will require a new acceptor labeling site on the N domain, because FITC blocks nucleotide binding. Future studies employing time-resolved FRET should have the sensitivity to detect distance heterogeneity (*70*) and thus test the Brownian motion hypothesis (*67*) for A−N domain distance and to test whether

the cytosolic domain of SERCA is closed throughout the catalytic cycle (*69*).

Conclusions. By constructing a CFP−SERCA fusion protein in insect cell microsomes, we have solved a long-standing problem: the lack of a specific fluorescent probe of the SERCA A domain. Measurements of ATPase activity and proteolytic susceptibility indicate that this construct undergoes Ca-dependent structural transitions similar to those of native SERCA. FRET measurements from this A-domain donor to a N-domain acceptor (FITC attached to Lys 515), coupled with molecular simulations, provide direct tests of models derived from crystal structures. These measurements give results in the absence of Ca that are consistent with the proposed compact structure of the cytosolic headpiece of SERCA. However, upon addition of Ca, only a slight separation of the probes occurs, indicating that the mean separation of the A and N domains is not as great as indicated by the E1−Ca crystal structure (1SU4). We conclude that either (a) the headpiece retains a compact structure throughout its catalytic cycle or (b) the Ca-bound E1 state is a dynamically disordered structure that samples both open and closed conformations, with an average structure that is only slightly different from the closed E2 structure.

REFERENCES

1. McIntosh, D. B., Woolley, D. G., MacLennan, D. H., Vilsen, B., and Andersen, J. P. (1999) Interaction of nucleotides with Asp[351] and the conserved phosphorylation loop of sarcoplasmic reticulum Ca²⁺−ATPase. *J. Biol. Chem. 274*, 25227–25236.
2. Clarke, D. M., Loo, T. W., Inesi, G., and MacLennan, D. H. (1989) Location of high affinity Ca²⁺-binding sites within the predicted transmembrane domain of the sarcoplasmic reticulum Ca²⁺−ATPase. *Nature 339*, 476–478.
3. Clarke, D. M., Loo, T. W., and MacLennan, D. H. (1990) Functional consequences of alterations to amino acids located in the nucleotide binding domain of the Ca²⁺−ATPase of sarcoplasmic reticulum. *J. Biol. Chem. 265*, 22223–22227.
4. Maruyama, K., and MacLennan, D. H. (1988) Mutation of aspartic acid-351, lysine-352, and lysine-515 alters the Ca²⁺ transport activity of the Ca²⁺−ATPase expressed in COS-1 cells. *Proc. Natl. Acad. Sci. U.S.A. 85*, 3314–3318.
5. MacLennan, D. H., Clarke, D. M., Loo, T. W., and Skerjanc, I. S. (1992) Site-directed mutagenesis of the Ca²⁺−ATPase of sarcoplasmic reticulum. *Acta Physiol. Scand. Suppl. 607*, 141–150.
6. Zhang, P., Toyoshima, C., Yonekura, K., Green, N. M., and Stokes, D. L. (1998) Structure of the calcium pump from sarcoplasmic reticulum at 8 Å resolution. *Nature 392*, 835–839.
7. Toyoshima, C., Sasabe, H., and Stokes, D. L. (1993) Three-dimensional cryo-electron microscopy of the calcium ion pump in the sarcoplasmic reticulum membrane. *Nature 362*, 467–471.
8. Stokes, D. L., Zhang, P., Toyoshima, C., Yonekura, K., Ogawa, H., Lewis, M. R., and Shi, D. (1998) Cryoelectron microscopy of the calcium pump from sarcoplasmic reticulum: Two crystal forms reveal two different conformations. *Acta Physiol. Scand. Suppl. 643*, 35–43.
9. Stokes, D. L., and Green, N. M. (1990) Three-dimensional crystals of Ca−ATPase from sarcoplasmic reticulum. Symmetry and molecular packing. *Biophys. J. 57*, 1–14.
10. Ogawa, H., Stokes, D. L., Sasabe, H., and Toyoshima, C. (1998) Structure of the Ca²⁺ pump of sarcoplasmic reticulum: A view along the lipid bilayer at 9 Å resolution. *Biophys. J. 75*, 41–52.
11. Boland, R., Martonosi, A., and Tillack, T. W. (1974) Developmental changes in the composition and function of sarcoplasmic reticulum. *J. Biol. Chem. 249*, 612–623.
12. Tillack, T. W., Boland, R., and Martonosi, A. (1974) The ultrastructure of developing sarcoplasmic reticulum. *J. Biol. Chem. 249*, 624–633.
13. Bigelow, D. J., Squier, T. C., and Inesi, G. (1992) Phosphorylation-dependent changes in the spatial relationship between Ca−ATPase polypeptide chains in sarcoplasmic reticulum membranes. *J. Biol. Chem. 267*, 6952–6962.
14. Bigelow, D. J., and Inesi, G. (1992) Contributions of chemical derivatization and spectroscopic studies to the characterization of the Ca²⁺ transport ATPase of sarcoplasmic reticulum. *Biochim. Biophys. Acta 1113*, 323–338.
15. Birmachu, W., Nisswandt, F. L., and Thomas, D. D. (1989) Conformational transitions in the calcium adenosinetriphosphatase studied by time-resolved fluorescence resonance energy transfer. *Biochemistry 28*, 3940–3947.
16. Lewis, S. M., and Thomas, D. D. (1992) Resolved conformational states of spin-labeled Ca−ATPase during the enzymatic cycle. *Biochemistry 31*, 7381–7389.
17. Mueller, B., Zhao, M., Negrashov, I. V., Bennett, R., and Thomas, D. D. (2004) SERCA structural dynamics induced by ATP and calcium. *Biochemistry 43*, 12846–12854.
18. Toyoshima, C., Nakasako, M., Nomura, H., and Ogawa, H. (2000) Crystal structure of the calcium pump of sarcoplasmic reticulum at 2.6 Å resolution. *Nature 405*, 647–655.
19. Toyoshima, C., and Nomura, H. (2002) Structural changes in the calcium pump accompanying the dissociation of calcium. *Nature 418*, 605–611.
20. Olesen, C., Sørensen, T. L., Nielsen, R. C., Møller, J. V., and Nissen, P. (2004) Dephosphorylation of the calcium pump coupled to counterion occlusion. *Science 306*, 2251–2255.
21. Sørensen, T. L., Møller, J. V., and Nissen, P. (2004) Phosphoryl transfer and calcium ion occlusion in the calcium pump. *Science 304*, 1672–1675.
22. Sørensen, T. L., Clausen, J. D., Jensen, A. M., Vilsen, B., Møller, J. V., Andersen, J. P., and Nissen, P. (2004) Localization of a K⁺-binding site involved in dephosphorylation of the sarcoplasmic reticulum Ca²⁺−ATPase. *J. Biol. Chem. 279*, 46355–46358.
23. Toyoshima, C., Nomura, H., and Tsuda, T. (2004) Lumenal gating mechanism revealed in calcium pump crystal structures with phosphate analogues. *Nature 432*, 361–368.
24. Toyoshima, C., and Mizutani, T. (2004) Crystal structure of the calcium pump with a bound ATP analogue. *Nature 430*, 529–535.
25. Møller, J. V., Olesen, C., Jensen, A. M., and Nissen, P. (2005) The structural basis for coupling of Ca²⁺ transport to ATP hydrolysis by the sarcoplasmic reticulum Ca²⁺−ATPase. *J. Bioenerg. Biomembr. 37*, 359–364.
26. Møller, J. V., Nissen, P., Sørensen, T. L., and le Maire, M. (2005) Transport mechanism of the sarcoplasmic reticulum Ca²⁺−ATPase pump. *Curr. Opin. Struct. Biol. 15*, 387–393.
27. Obara, K., Miyashita, N., Xu, C., Toyoshima, I., Sugita, Y., Inesi, G., and Toyoshima, C. (2005) Structural role of countertransport revealed in Ca²⁺ pump crystal structure in the absence of Ca²⁺. *Proc. Natl. Acad. Sci. U.S.A. 102*, 14489–14496.
28. Takahashi, M., Kondou, Y., and Toyoshima, C. (2007) Interdomain communication in calcium pump as revealed in the crystal structures with transmembrane inhibitors. *Proc. Natl. Acad. Sci. U.S.A. 104*, 5800–5805.
29. Toyoshima, C., and Inesi, G. (2004) Structural basis of ion pumping by Ca²⁺−ATPase of the sarcoplasmic reticulum. *Annu. Rev. Biochem. 73*, 269–292.
30. Cornea, R. L., Autry, J. M., Chen, Z., and Jones, L. R. (2000) Reexamination of the role of the leucine/isoleucine zipper residues of phospholamban in inhibition of the Ca²⁺ pump of cardiac sarcoplasmic reticulum. *J. Biol. Chem. 275*, 41487–41494.
31. Sagara, Y., and Inesi, G. (1991) Inhibition of the sarcoplasmic reticulum Ca²⁺ transport ATPase by thapsigargin at subnanomolar concentrations. *J. Biol. Chem. 266*, 13503–13506.
32. Dupont, Y., and Leigh, J. B. (1978) Transient kinetics of sarcoplasmic reticulum Ca²⁺ + Mg²⁺ ATPase studied by fluorescence. *Nature 273*, 396–398.
33. Gryczynski, I., Wiczk, W., Inesi, G., Squier, T., and Lakowicz, J. R. (1989) Characterization of the tryptophan fluorescence from sarcoplasmic reticulum adenosinetriphosphatase by frequency-domain fluorescence spectroscopy. *Biochemistry 28*, 3490–3498.

34. Pick, U., and Karlish, S. J. (1982) Regulation of the conformation transition in the Ca−ATPase from sarcoplasmic reticulum by pH, temperature, and calcium ions. *J. Biol. Chem. 257*, 6120–6126.

35. Pick, U., and Karlish, S. J. (1980) Indications for an oligomeric structure and for conformational changes in sarcoplasmic reticulum Ca^{2+}−ATPase labelled selectively with fluorescein. *Biochim. Biophys. Acta 626*, 255–261.

36. Jona, I., Matko, J., and Martonosi, A. (1990) Structural dynamics of the Ca^{2+}−ATPase of sarcoplasmic reticulum. Temperature profiles of fluorescence polarization and intramolecular energy transfer. *Biochim. Biophys. Acta 1028*, 183–199.

37. Corbalan-Garcia, S., Teruel, J. A., and Gomez-Fernandez, J. C. (1993) Intramolecular distances within the Ca^{2+}−ATPase from sarcoplasmic reticulum as estimated through fluorescence energy transfer between probes. *Eur. J. Biochem. 217*, 737–744.

38. Brandl, C. J., deLeon, S., Martin, D. R., and MacLennan, D. H. (1987) Adult forms of the Ca^{2+}−ATPase of sarcoplasmic reticulum. Expression in developing skeletal muscle. *J. Biol. Chem. 262*, 3768–3774.

39. Zhang, J., Campbell, R. E., Ting, A. Y., and Tsien, R. Y. (2002) Creating new fluorescent probes for cell biology. *Nat. Rev. Mol. Cell Biol. 3*, 906–918.

40. Autry, J. M., and Jones, L. R. (1997) Functional co-expression of the canine cardiac Ca^{2+} pump and phospholamban in *Spodoptera frugiperda* (Sf21) cells reveals new insights on ATPase regulation. *J. Biol. Chem. 272*, 15872–15880.

41. Fernandez, J. L., Rosemblatt, M., and Hidalgo, C. (1980) Highly purified sarcoplasmic reticulum vesicles are devoid of Ca^{2+}-independent ("basal") ATPase activity. *Biochim. Biophys. Acta 599*, 552–568.

42. Lowry, O. H., Rosebrough, N. J., Farr, A. L., and Randall, R. J. (1951) Protein measurement with the folin phenol reagent. *J. Biol. Chem. 193*, 265–275.

43. Reddy, L. G., Cornea, R. L., Winters, D. L., McKenna, E., and Thomas, D. D. (2003) Defining the molecular components of calcium transport regulation in a reconstituted membrane system. *Biochemistry 42*, 4585–4592.

44. Fabiato, A., and Fabiato, F. (1979) Calculator programs for computing the composition of the solutions containing multiple metals and ligands used for experiments in skinned muscle cells. *J. Physiol. (Paris) 75*, 463–505.

45. Danko, S., Yamasaki, K., Daiho, T., Suzuki, H., and Toyoshima, C. (2001) Organization of cytoplasmic domains of sarcoplasmic reticulum Ca^{2+}−ATPase in E$_1$P and E$_1$ATP states: A limited proteolysis study. *FEBS Lett. 505*, 129–135.

46. Danko, S., Daiho, T., Yamasaki, K., Kamidochi, M., Suzuki, H., and Toyoshima, C. (2001) ADP-insensitive phosphoenzyme intermediate of sarcoplasmic reticulum Ca^{2+}−ATPase has a compact conformation resistant to proteinase K, V8 protease and trypsin. *FEBS Lett. 489*, 277–282.

47. Tsien, R. Y. (1998) The green fluorescent protein. *Annu. Rev. Biochem. 67*, 509–544.

48. Stryer, L. (1978) Fluorescence energy transfer as a spectroscopic ruler. *Annu. Rev. Biochem. 47*, 819–846.

49. Dale, R. E., Eisinger, J., and Blumberg, W. E. (1979) The orientational freedom of molecular probes. The orientation factor in intramolecular energy transfer. *Biophys. J. 26*, 161–193.

50. Budisa, N., Pal, P. P., Alefelder, S., Birle, P., Krywcun, T., Rubini, M., Wenger, W., Bae, J. H., and Steiner, T. (2004) Probing the role of tryptophans in *Aequorea victoria* green fluorescent proteins with an expanded genetic code. *Biol. Chem. 385*, 191–202.

51. Chaing, J., Li, I., Pham, E., and Truong, K. (2006) FPMOD: A modeling tool for sampling the conformational space of fusion proteins, Proceedings of 28th Annual International IEEE Engineering Conference in Medicine and Biology.

52. Pham, E., Chiang, J., Li, I., Shum, W., and Truong, K. (2007) A computational tool for designing FRET protein biosensors by rigid-body sampling of their conformational space. *Structure 15*, 515–523.

53. Humphrey, W., Dalke, A., and Schulten, K. (1996) VMD: Visual molecular dynamics. *J. Mol. Graphics14*, 33–38, 27–28.

54. Rosell, F. I., and Boxer, S. G. (2003) Polarized absorption spectra of green fluorescent protein single crystals: Transition dipole moment directions. *Biochemistry 42*, 177–183.

55. Lettinga, M. P., Zuilhof, H., and van Zandvoort, M. A. M. J. (2000) Phosphorescence and fluorescence characterization of fluorescein derivatives immobilized in various polymer matrices. *Phys. Chem. Chem. Phys. 2*, 3697–3707.

56. Autry, J. M., and Jones, L. R. (1998) High-level coexpression of the canine cardiac calcium pump and phospholamban in Sf21 insect cells. *Ann. N.Y. Acad. Sci. 853*, 92–102.

57. Karon, B. S., Autry, J. M., Shi, Y., Garnett, C. E., Inesi, G., Jones, L. R., Kutchai, H., and Thomas, D. D. (1999) Different anesthetic sensitivities of skeletal and cardiac isoforms of the Ca−ATPase. *Biochemistry 38*, 9301–9307.

58. Waggoner, J. R., Huffman, J., Griffith, B. N., Jones, L. R., and Mahaney, J. E. (2004) Improved expression and characterization of Ca^{2+}−ATPase and phospholamban in High-Five cells. *Protein Expression Purif. 34*, 56–67.

59. Squier, T. C., Bigelow, D. J., Garcia de Ancos, J., and Inesi, G. (1987) Localization of site-specific probes on the Ca−ATPase of sarcoplasmic reticulum using fluorescence energy transfer. *J. Biol. Chem. 262*, 4748–4754.

60. Inesi, G., Ma, H., Hua, S., and Toyoshima, C. (2003) Characterization of Ca^{2+}−ATPase residues involved in substrate and cation binding. *Ann. N.Y. Acad. Sci. 986*, 63–71.

61. Juul, B., Turc, H., Durand, M. L., Gomez de Gracia, A., Denoroy, L., Møller, J. V., Champeil, P., and le Maire, M. (1995) Do transmembrane segments in proteolyzed sarcoplasmic reticulum Ca^{2+}−ATPase retain their functional Ca^{2+} binding properties after removal of cytoplasmic fragments by proteinase K? *J. Biol. Chem. 270*, 20123–20134.

62. Inesi, G., Lewis, D., Toyoshima, C., Hirata, A., and de Meis, L. (2007) Conformational fluctuations of the Ca^{2+}−ATPase in the native membrane environment. Effects of pH, temperature, catalytic substrates, and thapsigargin. *J. Biol. Chem. 283*, 1189–1196.

63. Rocheleau, J. V., Edidin, M., and Piston, D. W. (2003) Intrasequence GFP in class I MHC molecules, a rigid probe for fluorescence anisotropy measurements of the membrane environment. *Biophys. J. 84*, 4078–4086.

64. Sohoel, H., Jensen, A. M., Møller, J. V., Nissen, P., Denmeade, S. R., Isaacs, J. T., Olsen, C. E., and Christensen, S. B. (2006) Natural products as starting materials for development of second-generation SERCA inhibitors targeted towards prostate cancer cells. *Bioorg. Med. Chem. 14*, 2810–2815.

65. Champeil, P., Menguy, T., Soulie, S., Juul, B., de Gracia, A. G., Rusconi, F., Falson, P., Denoroy, L., Henao, F., le Maire, M., and Møller, J. V. (1998) Characterization of a protease-resistant domain of the cytosolic portion of sarcoplasmic reticulum Ca^{2+}−ATPase. Nucleotide- and metal-binding sites. *J. Biol. Chem. 273*, 6619–6631.

66. Krebs, W. G., and Gerstein, M. (2000) The morph server: A standardized system for analyzing and visualizing macromolecular motions in a database framework. *Nucleic Acids Res. 28*, 1665–1675.

67. Xu, C., Rice, W. J., He, W., and Stokes, D. L. (2002) A structural model for the catalytic cycle of Ca^{2+}−ATPase. *J. Mol. Biol. 316*, 201–211.

68. Sørensen, T. L., Olesen, C., Jensen, A. M., Møller, J. V., and Nissen, P. (2006) Crystals of sarcoplasmic reticulum Ca^{2+}−ATPase. *J. Biotechnol. 124*, 704–716.

69. Jensen, A. M., Sørensen, T. L., Olesen, C., Møller, J. V., and Nissen, P. (2006) Modulatory and catalytic modes of ATP binding by the calcium pump. *EMBO J. 25*, 2305–2314.

70. Haas, E., Wilchek, M., Katchalski-Katzir, E., and Steinberg, I. Z. (1975) Distribution of end-to-end distances of oligopeptides in solution as estimated by energy transfer. *Proc. Natl. Acad. Sci. U.S.A. 72*, 1807–1811.